1 **Title**

2 A touch of hierarchy. Population Receptive Fields reveal fingertip integration in Brodmann

3 areas in human primary somatosensory cortex.

4

5 **Authors**

6 W. Schellekens[1], M. Thio[1], S. Badde[2], J. Winawer[2], N. Ramsey[3], N. Petridou[1]

7

8 **Affiliations**

9 1: Department of Radiology, Center for Image Sciences, UMC Utrecht, Utrecht, Netherlands

10 2: Department of Psychology & Center of Neural Science, NYU, New York, USA

11 3: Department of Neurology & Neurosurgery, UMC Utrecht, Utrecht, Netherlands

12

13 **Corresponding author**

14 W. Schellekens

15 Postal address:

16 Q101.132, P.O.Box 85500, 3508 GA, Utrecht, Netherlands

17 e-mail address:

18 w.schellekens@umcutrecht.nl

19

Abstract

Several neuroimaging studies have shown the somatotopy of body part representations in primary somatosensory cortex (S1), but the functional hierarchy of distinct subregions in human S1 has not been adequately addressed. The current study investigates the functional hierarchy of cyto-architectonically distinct regions, Brodmann areas BA3, BA1, and BA2, in human S1. During functional MRI experiments, we presented participants with vibrotactile stimulation of the fingertips at 3 different vibration frequencies. Using population Receptive Field (pRF) modeling of the fMRI BOLD activity, we identified the hand region in S1 and the somatotopy of the fingertips. For each voxel, the pRF center indicates the finger that most effectively drives the BOLD signal, and the pRF size measures the spatial somatic pooling of fingertips. We find a systematic relationship of pRF sizes from lower-order areas to higher-order areas. Specifically, we found that pRF sizes are smallest in BA3, increase slightly towards BA1, and are largest in BA2, paralleling the increase in visual receptive field size as one ascends the visual hierarchy. Additionally, we find that the time-to-peak of the hemodynamic response in BA3 is roughly 0.5s earlier compared to BA1 and BA2, further supporting the notion of a functional hierarchy of subregions in S1. These results were obtained during stimulation of different mechanoreceptors, suggesting that different afferent fibers leading up to S1 feed into the same cortical hierarchy.

Keywords

Somatosensory; S1; fMRI; pRF; hierarchy; vibrotactile

Introduction

40

41 Touch is an important source of information on our direct surroundings. We use touch

42 information to explore objects and surfaces and touch plays a major part in haptic processes

43 such as tool use. The loss of adequate touch signal processing, e.g. due to stroke, frequently

44 leads to severe impairments affecting many facets of everyday life. Hence, understanding

45 somatosensory processes in the human brain following cutaneous touch signals is relevant

46 to many scientific areas ranging from fundamental neuroscience to the deciphering of

47 neurological disorders of the somatosensory system. Imaging studies in humans have mostly

48 addressed the somatotopic organization of the hand and fingers (Maldjian et al. 1999; Kurth

49 et al. 2000; Hlustík et al. 2001; Blankenburg et al. 2003; Nelson and Chen 2008; Schweizer

50 et al. 2008; Sanchez-Panchuelo et al. 2010; Ann Stringer et al. 2014; Martuzzi et al. 2014;

51 Choi et al. 2016; Kikkert et al. 2016; Kolasinski et al. 2016; Sanchez Panchuelo et al. 2018;

52 Da Rocha Amaral et al. 2019; Puckett et al. 2020), and the whole body (Akselrod et al. 2017;

53 Tal et al. 2017). However, other functional characteristics of human S1 have not received

54 equal attention. Specifically, the processing hierarchy of cyto-architectonically distinct regions

55 in human S1, i.e. Brodmann areas BA3a/b, BA1, and BA2, (Brodmann 1909; Geyer et al.

56 1999), has been investigated structurally in humans (Sánchez-Panchuelo et al. 2014;

57 Wagstyl et al. 2015), but not from a functional perspective. In the current study, we

58 investigate the functional hierarchy in human S1 by estimating the integration of somatic

59 information in different Brodmann areas.

60   When cortical information is processed at different hierarchical levels, information

61 from multiple lower-level sources is integrated at the higher-order level. As a result, regions

62 of higher hierarchical order contain neurons that exhibit larger or more complex receptive

63 fields, meaning that neurons are responsive to more input or specific combinations of input.

64 Functional hierarchy among separate S1 regions in humans can, therefore, potentially be

65 revealed through a form of spatial somatosensory information integration (Hubel and Wiesel

66 1968; Duffy and Burchfiel 1971; Van Essen and Maunsell 1983). Previous animal studies

67 have reported that BA3b is the primary target of thalamic output from the ventrolateral and

68 ventroposterior nucleus (Jones and Powell 1970; Chung et al. 1986; Miller et al. 2001), which

69 then projects onwards to BA1 and BA2 (Friedman 1983; Felleman and Van Essen 1991;

70 Kaas 1993; Iwamura 1998). As a result, neuronal receptive fields, as reported in animal

71 studies, are smallest in BA3b and increase in size in BA1, BA2 and beyond (Armstrong-

72 James 1975; Hyvärinen and Poranan 1978; Sur et al. 1980; DiCarlo et al. 1998). In humans,

73 receptive field properties of individual neurons cannot easily be assessed in healthy

74 volunteers under normal circumstances. However, average receptive field properties of small

75 neuronal populations (e.g. neurons inside a single MRI-voxel) can be estimated using a

76 Gaussian population Receptive Field (pRF) model. PRF modeling was originally developed

77 for vision (Dumoulin and Wandell 2008), where it has exposed hierarchical processing

78 characteristics as well as other traits of the human visual system (Harvey and Dumoulin

79 2011; Haak et al. 2012; Dumoulin et al. 2014; Klein et al. 2014; Wandell and Winawer 2015;

80 Merkel et al. 2018; Welbourne et al. 2018). Furthermore, two recent functional MRI (fMRI)

81 studies have shown that pRF modeling can also be used to describe the average receptive

82 field properties of small neuronal populations in human S1 (Schellekens et al. 2018; Puckett

83 et al. 2020). Even though some studies find evidence consistent with hierarchical

84 organization of somatosensory processing in humans (Bodegård et al. 2001; Van Boven et

85 al. 2005; Dijkerman and de Haan 2007; Kim et al. 2015; Whitehead et al. 2019), the extent of

86 spatial integration across different Brodmann areas in human S1 is presently not well

87 defined.

88 The current objective is to estimate pRF properties across Brodmann areas, following

89 vibrotactile stimulation of the fingertips. Vibrotactile stimulation can be signaled by two

90 distinct cutaneous mechanoreceptors: Meissner corpuscles and Pacinian corpuscles,

91 depending on the frequency of vibration (Mountcastle et al. 1972; Bolanowski et al. 1988;

92 Pasterkamp 1999). Meissner corpuscles typically show a peak activity for flutter frequencies

93 (i.e. between 10 Hz and 50 Hz), while Pacinian corpuscles respond to higher frequencies

94 with a preference around 250 Hz (Rowe 2002). Furthermore, previous studies showed that

95 Meissner and Pacinian corpuscles signal somatosensory information through different

96 pathways, i.e. Rapid-Adapting (RA) and Pacinian pathways (Vallbo and Johansson 1984;

97 Gescheider et al. 2004; Harvey et al. 2013; Saal et al. 2015), which reportedly project to

98 different regions of the thalamus (Herron and Dykes 1986; Kaas 1993). Additionally, Pacinian

99 pathways may have more connections to BA1 than BA3b (Paul et al. 1972; Hyvärinen and

100 Poranan 1978; Iwamura et al. 1993). Hence, the hierarchical order of somatosensory

101 processing among Brodmann areas in S1 may be frequency-dependent or at least influenced

102 by the supplied frequency of vibration. To investigate hierarchical differences caused by

103 stimulated mechanoreceptor type, we supplied a vibrational stimulus to the fingertips at three

104 different frequencies: 30 Hz, 110 Hz, and 190 Hz. A perfect isolation of stimulated

105 mechanoreceptor type is not realistic and multiple pathways likely contribute to the observed

106 cortical signal with increasing contributions of Pacinian pathways for higher stimulation

107 frequencies (Choi et al. 2016; Kuroki et al. 2017). Thus, differences in initial cortical

108 projection site between RA an Pacinian pathways could be detected through changes in pRF

109 size for different vibrotactile stimulation frequencies.

110 In the present study, we scrutinize the hierarchical organization of S1 by measuring

111 the properties of tactile pRFs in BA3b (from here on referred to as BA3), BA1, and BA2. The

4

112   five fingers of the right hand were vibrotactually stimulated at three different frequencies, 30

113   Hz, 110 Hz, and 190 Hz, while Blood-Oxygen-Level-Dependent (BOLD) activity in S1 was

114   measured with 7T fMRI. PRF modeling allows us to infer the somatotopic tuning of neuronal

115   populations in each of the three Brodmann areas. We expect an increase in pRF size, the

116   specificity of the somatotopic tuning, along the somatosensory processing pathway. Such a

117   finding would indicate increasing spatial integration and be in accordance with sequential

118   information processing and increasing processing complexity from BA3 to BA1, and finally

119   BA2. The hierarchical order across Brodmann areas is further investigated by examining the

120   temporal dynamics of the hemodynamic response function (HRF). Finally, the effect of

121   mechanoreceptor pathway on cortical pRF size is presently unknown. Through pRF size

122   estimations in different Brodmann areas under different vibrotactile frequency conditions, we

123   investigate putative differences in cortical hierarchical projections related to different

124   mechanoreceptor types.

125 **Material & Methods**

126 *Participants*

127 Eight healthy volunteers (age range 23-31 years old, 4 female) participated in the study. All

128 participants gave written informed consent before entering the study. The protocol was

129 approved by the local medical ethics committee of the University Medical Center Utrecht,

130 Netherlands, in accordance with the Declaration of Helsinki (2013).

131 *Apparatus*

132 The vibrotactile stimulus was delivered using MR-compatible piezoelectric stimulators with a

133 triangular shaped tip and a contact area of approximately 1 mm^2 (http://dancerdesign.co.uk/).

134 The stimulation was controlled via a custom-written MATLAB (www.mathworks.com) script.

135 Analog stimulus signals were transferred to the stimulators using a NI-9264 digital-to-analog

136 converter output module (National Instruments, Austin, TX, USA), which was connected to a

137 conventional laptop and an amplifier.

138 We mounted 5 stimulators on a plexiglass plate using ordinary adhesive gum. The

139 adhesive gum allowed for the repositioning of the 5 stimulators to match each participant's

140 hand. The fingertips of the right hand were placed on the stimulators (digits did not touch

141 each other). The hand and fingers were taped to the plexiglass plate with standard paper

142 tape to prevent the fingers from accidentally disconnecting from the stimulators. The

143 plexiglass plate rested on the participant's abdomen, while the right elbow was supported by

144 towels. Using this setup, the subject could maintain a stationary position of the right

145 arm/hand comfortably for the full length of the fMRI experiments. This minimized movement

146 of the hands, which could affect the results. Moreover, subjects were explicitly instructed to

147 keep both hands still during the experiments.

148 *Procedure and stimuli*

149 Each subject underwent 4 fMRI experiments: the first 3 were pRF experiments, conducted to

150 estimate pRF properties (i.e. receptive field center, size, and amplitude). These 3

151 experiments differed only with respect to the frequency of vibration (30 Hz, 110 Hz, and 190

152 Hz). The 4th fMRI experiment was conducted to estimate the hemodynamic response

153 function (HRF) within each individual subject's S1. During the 3 pRF experiments, each

154 fingertip was stimulated 8 times in a pseudo-randomized order. Only one fingertip was

155 stimulated at a time, and a single stimulation lasted for 4s. An intermittent stimulation

156 paradigm was chosen to minimize adaptation processes and, therefore, maximize the

157 observed BOLD response: during the 4s stimulation period, a 400ms on period was

6

158   alternated with a 100ms off period. After the 4s stimulation period, a 10s rest period ensued

159   except for 8 randomly selected stimulation periods when the ensuing rest period was

160   lengthened to 14.4s. Our analysis did not require a complete return to baseline, but rather

161   allowed for the response to one stimulus to persist into the onset of the next. In total, a single

162   pRF experiment took 595.2s. During the HRF experiment, a brief vibrotactile stimulation of

163   500ms at 30 Hz was applied to all 5 fingertips simultaneously. The brief 500ms stimulation

164   was delivered intermittently: 200ms on / 100ms off / 200ms on. There were 32 500ms events

165   throughout the HRF experiment with variable inter-stimulus interval (ISI). The minimum ISI

166   was 3.05s, the maximum ISI was 23.97s, and the median ISI was 7.98s.The full HRF

167   experiment took 320s.

168   *Scan protocol*

169   Scanning was conducted at a 7 Tesla Philips Achieva scanner (Philips, Best, Netherlands),

170   using a volume transmit and a 32-channel receive headcoil (Nova medical, MA, USA). A

171   multi-slice gradient echo (GE) echo-planar imaging (EPI) sequence was used for functional

172   image acquisition with the following specifications: TR/TE: 1600/27ms, flip angle: 70°,

173   SENSE factor: 3 in the anterior-posterior direction, field-of view (FOV) (ap,fh,rl): 209.4 x 41.6

174   x 165.0 mm at 1.6 x 1.6 x 1.6 mm voxel resolution, and interleaved slice acquisition. The

175   FOV was placed on the superior part of the brain, covering the hand region of the postcentral

176   gyrus. 372 volumes were acquired per pRF experiment and 200 volumes were acquired for

177   the HRF experiment. Additionally, 10 volumes were acquired with a reversed phase

178   encoding direction (i.e. posterior to anterior) for correction of geometrical distortions. Finally,

179   a whole-brain T1-weighted volume was acquired with TR/TE: 7.00/3.05ms, flip angle: 8°,

180   FOV (ap,fh,rl): 250 x 200 x 190 mm at 0.78 x 0.78 x 0.8 mm voxel size, and a whole-brain

181   proton density volume of equal dimensions.

182   *Image processing*

183   The T1-weighted anatomical volume was adjusted for proton density to correct for large

184   scale intensity inhomogeneities (Van de Moortele et al. 2009). Afterwards white matter and

185   pial brain surfaces were estimated using Freesurfer (https://surfer.nmr.mgh.harvard.edu/).

186   These surfaces were also inflated and flattened using Freesurfer. The functional volumes

187   were slice time corrected, realigned (i.e. corrected for head motion), corrected for

188   geometrical distortions, and co-registered to the anatomical T1-weighted volume using AFNI.

189   Transformation matrices for these steps were computed using the AFNI functions 3dvolreg,

190   3dQwarp, and 3dAllineate, respectively. The transformation matrices were combined and all

191   spatial preprocessing transformations were applied within a single interpolation step using

192   the AFNI function 3dNwarpApply to minimize smoothing caused by multiple interpolation

7

193   steps and general interpolation errors. The functional volumes were mapped onto the

194   estimated cortical surface reconstructions across the full depth of the estimated grey matter

195   using Freesurfer, creating a timeseries per surface vertex. The timeseries were high-pass

196   filtered with a cut-off at 0.01 Hz and rescaled to percent signal change. Finally, regions of

197   interest were drawn on the reconstructed cortical surface, based on the Brodmann area atlas

198   supplied by Freesurfer (Fischl et al. 2008). Region BA3 corresponded with atlas areas BA3a

199   and BA3b (covering the rostral wall of the postcentral gyrus). Region BA1 corresponded with

200   atlas area BA1 (covering the crown of the postcentral gyrus). Finally, region BA2 (covering

201   the caudal wall of the postcentral gyrus) was based on atlas area BA2, but manually limited

202   posteriorly at the base of the postcentral sulcus.

203   *pRF analysis*

204   Each vertex' timeseries was fitted with a Gaussian receptive field model, which described the

205   signal amplitude for any fingertip stimulation (1):

206    $g(x_i) = \exp\left(-\frac{(x_0-x_i)^2}{2 \cdot \sigma^2}\right), x_i \in N, x_0 \in \{\mathbb{R}_{>0.5} | \mathbb{R}_{<5.5}\}, \sigma \in \{\mathbb{R}_{>0}\}$ (1)

207   Where "x_i" represents the stimulated fingertip and "N" is the list of fingertips ranging from

208   1=thumb to 5=little finger. The estimated pRF center, "x_0", describes the preferred fingertip

209   per surface vertex and can be any real number (including fractioned numbers) between 0.5

210   and 5.5. A surface vertex is taken to prefer: the thumb when, 0.5<"x_0"<1.5, index finger when,

211   1.5<"x_0"<2.5, middle finger when, 2.5<"x_0"<3.5, ring finger when, 3.5<"x_0"<4.5, and the little

212   finger when, 4.5<"x_0"<5.5. The estimated pRF size, "σ", is the spread of the Gaussian in units

213   of fingers: the larger the pRF size, the more the neuronal population responds to stimulated

214   fingertips in addition to the preferred one. The receptive field model "$g(x_i)$", then, is used to

215   construct the effective task design (2):

216    $r(t) = \sum_{i \in N} s(x_i, t) \cdot g(x_i)$ (2)

217   Where "$r(t)$" is the effective task design, "$s(x_i,t)$" is the onset design matrix, which is a 2D

218   binary matrix representing for each fingertip "x_i" the stimulation onset and duration in scans

219   "t". The multiplication of the onset design matrix "$s(x_i,t)$" and the Gaussian receptive field

220   model "$g(x_i)$" is summed over the fingertip dimension, resulting in the effective task design

221   "$r(t)$". The effective task design is convolved with a hemodynamic response function (HRF),

222   resulting in the predicted timeseries (3):

223    $p(t) = r(t) * h(t)$ (3)

8

224 Where, "*h(t)*" is the HRF. Instead of assuming a canonical HRF, we convolved the estimated

225 HRFs from the HRF experiment (averaged across subjects, see below) with the effective

226 task design "*r(t)*". Therefore, we used an HRF that was specific for each Brodmann area. The

227 predicted timeseries model *"p(t)"* was compared with the measured timeseries of each vertex

228 (4):

229 $y(t) = \beta \cdot p(t) + c$ (4)

230 Where *y(t)* is the measured vertex' timeseries, "*p(t)*" is the predicted timeseries, "*β*" is a

231 scalar representing the signal amplitude and "*c*" is a constant. During the fitting procedure,

232 optimal fits are calculated for the pRF center "x_0" and size "*σ*" from equation (1) and "*β*" and

233 "*c*" from equation (4) using the Levenberg-Marquardt (Markwardt 2009) least-square

234 minimization algorithm (Figure 1). Finally, goodness-of-fit F-statistics were calculated for

235 each surface vertex model fit.
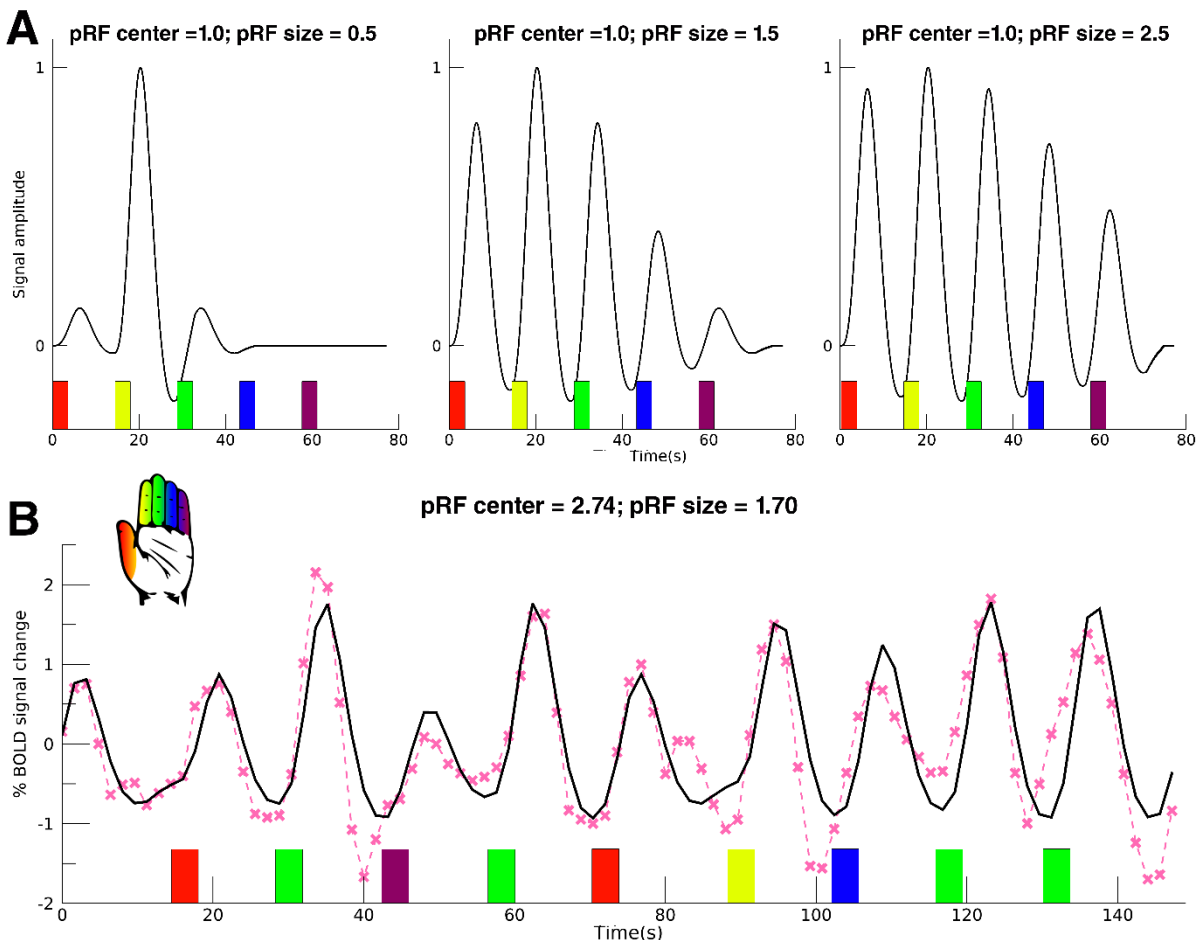
236

237 Figure 1

238 Title: pRF model timeseries

9

239 (A) Figure shows the effect of increasing pRF size on modeled timeseries. Left image shows model with pRF center = 1 (index

240 finger, yellow bar), pRF size = 0.5 (finger units). Middle image: pRF center = 1, pRF size = 1.5. Right image: pRF center = 1,

241 pRF size = 2.5. The model timeseries are convolved with the average HRF from the HRF experiment and the colored bars

242 denote the model onset time for each of the fingertip conditions, see hand icon. (B) Fitted pRF timeseries (black) for one

243 example vertex and the corresponding acquired fMRI timeseries (pink) are shown. For visibility, only a part of the complete

244 timeseries is shown. The onsets of the fingertip stimulation conditions are represented by the colored bars, see also hand icon.

245 This particular vertex was acquired from subject 4, BA1, 190 Hz, and was fitted with a model with pRF center= 2.74 (between

246 index and middle finger) and pRF size = 1.70 finger units.

HRF analysis

248 For the HRF experiment, we estimated the hemodynamic response function of each vertex

249 using a set of finite impulse response (FIR) functions (Lindquist et al. 2009). The timeseries

250 were upsampled by a factor of 4 using a 3th degree B-spline interpolation, resulting in a time

251 point every 400ms. This matched the stimulus onset resolution, as stimulus onsets were

252 locked to time samples every 400ms. A set of finite impulses were constructed to cover the

253 range of 14.4 seconds (i.e. 36 finite impulses), starting from the moment of stimulation. The

254 amplitude in percent signal change at each time point was calculated using a multiple linear

255 regression. An HRF per ROI was created by averaging the estimated HRFs of all vertices

256 within the ROIs that showed a significant fit with respect to the HRF task design (false-

257 discovery-rate corrected). Afterwards, the peak amplitude, time to peak (TTP) and full-width-

258 at-half-maximum (FWHM) were extracted from the estimated HRF curves.

Statistical analyses

260 For the statistical analyses of all experiments we included the surface vertices with a

261 significant goodness-of-fit F-statistic derived from the pRF experiments (false-discovery-rate

262 corrected) that fell in one of the three predefined ROIs. The percentage explained variance

263 per vertex was calculated through the Pearson correlation coefficient of predicted timeseries

264 and obtained timeseries squared. The presence of a somatotopy was assessed using the

265 vertex coordinates of the flattened surfaces. Initially, the flattened surfaces were manually

266 rotated so that the central sulcus was vertically aligned along the dorsoventral axis. A

267 somatotopy is defined here as the linear relationship between dorsoventral coordinates and

268 pRF centers. Hence, the slope between coordinates and pRF centers reflects the presence

269 of a somatotopy and was calculated using a linear regression per ROI, per vibrotactile

270 frequency and per subject. We used Student's t-test to test if slopes deviated significantly

271 from zero. We used a 2-way univariate repeated measures ANOVA with the slopes as

272 dependent variable and ROI and vibrotactile frequency as repeated measures factors (3

273 levels each) to test for differences in somatotopic structures per ROI or frequency of

274 vibration. The pRF sizes were binned in 5 preferred finger representation bins, according to

275 the pRF centers. Then, we applied a 3-way univariate repeated measures ANOVA to test for

276   differences in pRF size across ROI, vibrotactile frequency, and preferred finger

277   representation (with 3, 3, and 5 levels, respectively) with linear contrasts for each factor. The

278   same 3-way univariate repeated measures ANOVA was performed on the estimated

279   amplitude of the percent BOLD signal change (i.e. "β" from equation (4)). For the HRF

280   experiment, differences in peak amplitude, TTP, and FWHM per ROI were also tested for

281   using univariate repeated measures ANOVAs with only ROI as factor (3 levels).

Results

S1 Somatotopy – spatial organization of pRFs

We used a Gaussian receptive field model to estimate the timeseries of the pRF experiments (Figure 1B). The predicted timeseries explained on average 35% (s.d.=11%) of variance of the recorded BOLD fMRI signal within the 3 predefined ROIs. On the basis of the estimated pRF centers we found the somatotopy of the five fingertips along the ventrolateral to mediodorsal axis of the postcentral gyrus in all 3 Brodmann areas (Figure 2): BA3: $t_{(7)}$=13.10, p<0.001, BA1: $t_{(7)}$=13.25, p<0.001, BA2: $t_{(7)}$=8.51, p<0.001. The somatotopy, characterized as the slope of cortical coordinates and pRF centers, differed significantly across the 3 Brodmann areas ($F_{(2,14)}$=15.26, p<0.001). Particularly, the somatotopy was less clear in Brodmann area BA2 (post-hoc somatotopy slope t-tests BA3-BA1: $t_{(7)}$=0.55, p=0.589; BA3-BA2: $t_{(7)}$=5.04, p<0.001; BA1-BA2: $t_{(7)}$=4.48, p=0.001). In BA2 there appears to be a cluster of pRF centers for the thumb and index finger and a second cluster for the middle, ring and little fingers (Figure 2B). The frequency of vibration, however, did not influence the somatotopy slope ($F_{(2,14)}$=0.25, p=0.782), although the projected somatotopy appeared less clear in several participants during the 30 Hz vibration condition compared to higher frequencies (Figure 3). We, finally, did not observe an interaction effect between Brodmann areas and applied frequency of vibration on the somatotopy slope ($F_{(4,28)}$=0.85, p=0.505), meaning that we did not find evidence for a somatotopy change in any Brodmann area for higher frequencies.

12
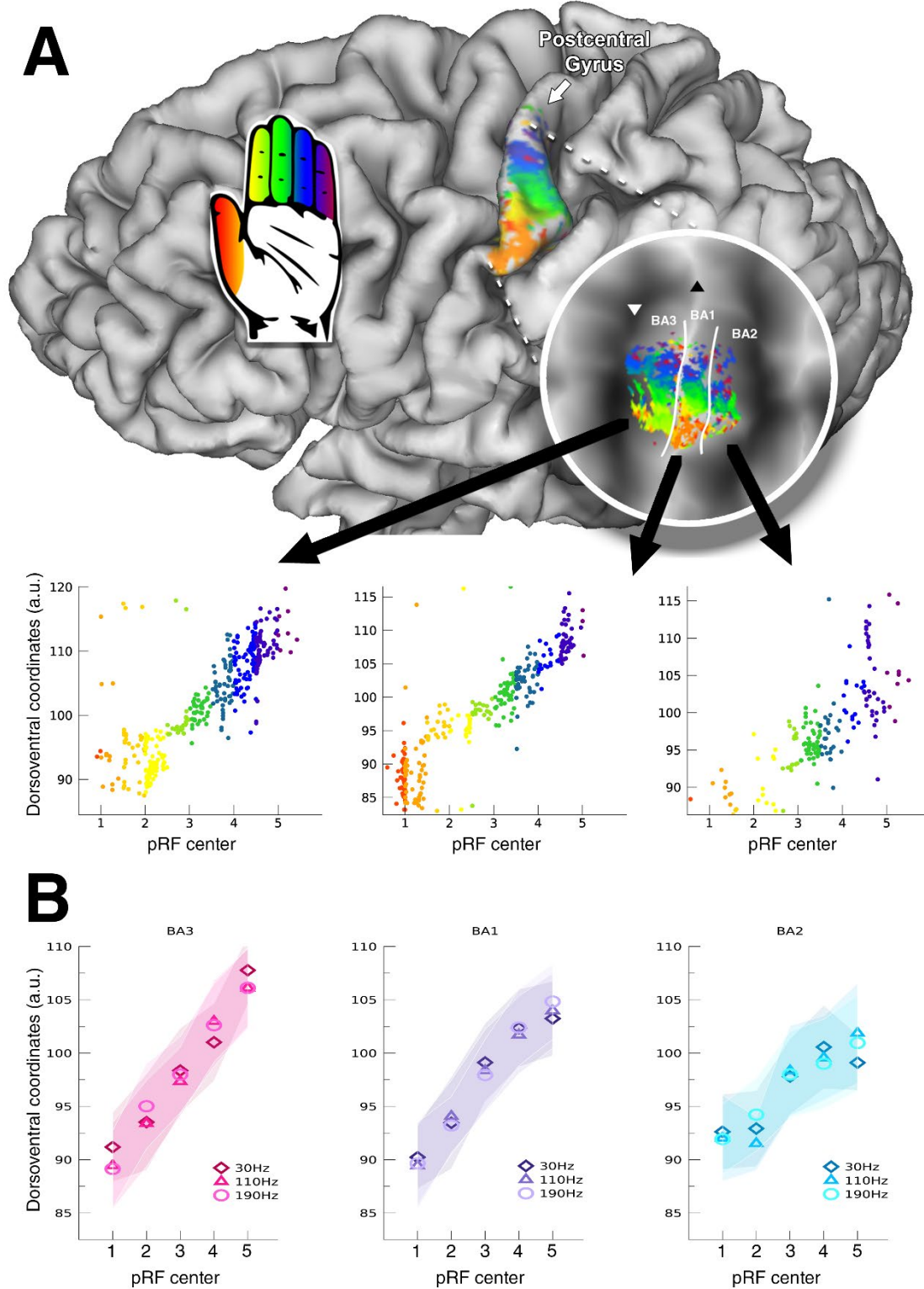
302

303 Figure 2

304 Title: Fingertip somatotopy

305 (A) Single subject pRF centers following 190 Hz vibrotactile stimulation are presented on a pial surface and flattened surface
306 (circle). The cortical coordinates along the dorsoventral axis plotted against the pRF centers are shown for all three Brodmann
307 areas. For the pRF centers, 1=thumb, 2=index finger, 3=middle finger, 4=ring finger, 5=little finger, which is also indicated by the
308 colors in the scatterplot and the hand icon. (B) Group average of cortical coordinates along the dorsoventral axis plotted against

13

309　　the mean pRF center per fingertip 1=thumb, 2=index finger, 3=middle finger, 4=ring finger, 5=little finger). Shaded area represents

310　　standard error of the mean across subjects. Different symbols represent different vibrational frequencies.
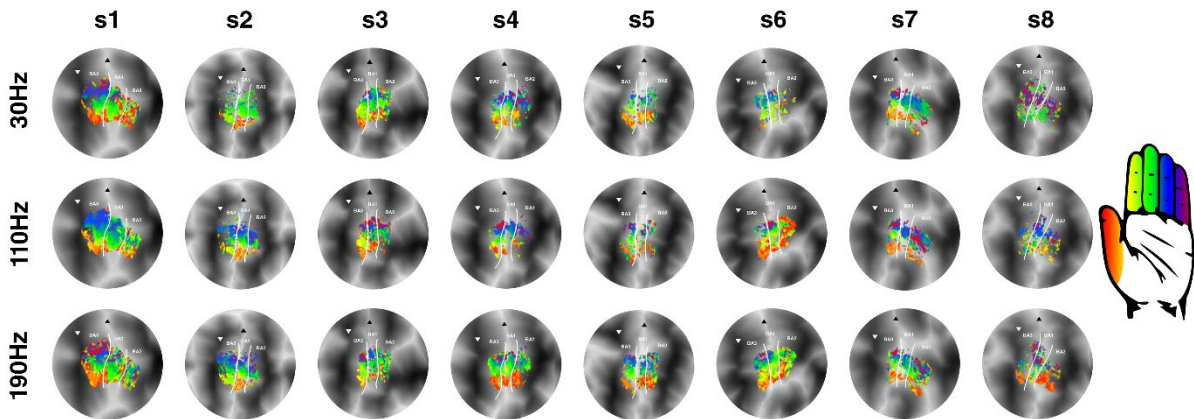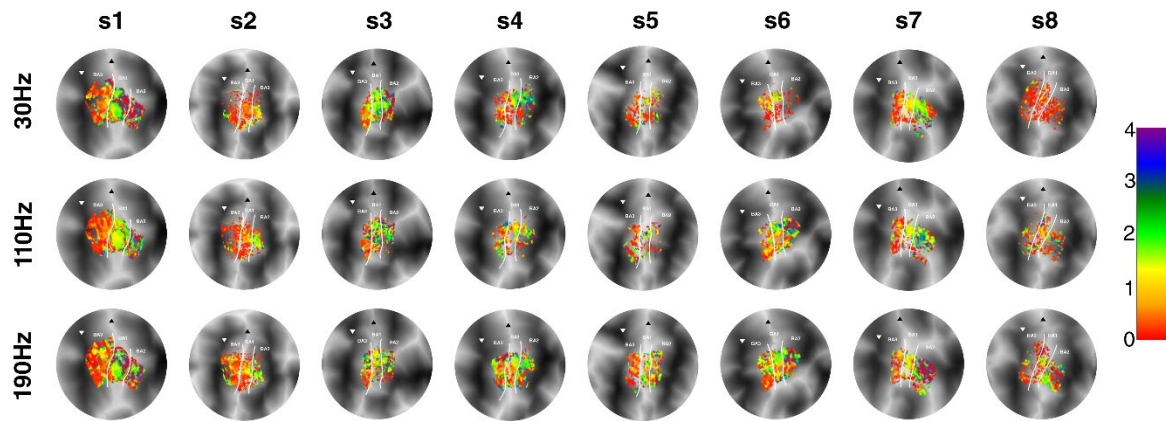

311

312　　Figure 3

313　　Title: pRF center maps

314　　The pRF centers are displayed on flattened cortical surfaces for all subjects (s1-s8). Rows depict the different frequencies of

315　　vibrotactile stimulation (30 Hz, 110 Hz & 190 Hz). Borders between Brodmann areas are denoted by the white solid line. The

316　　base of the central sulcus is shown by the white downward triangle, and the crown of the postcentral gyrus is indicated by the

317　　black upward triangle. Correspondence of pRF center and fingertip is denoted by the hand icon.

pRF sizes – fingertip specificity of the pRFs

319　　The estimated pRF sizes (Figure 4) differed significantly across Brodmann areas

320　　($F_{(2.14)}$=13.26, p<0.001), showing a significant linear increase ($t_{(14)}$=4.90, p<0.001) from BA3

321　　to BA1 and finally BA2 (Figure 5A). The frequency of vibrotactile stimulation also influenced

322　　the receptive field sizes ($F_{(2,14)}$=6.03, p=0.013, figure 5B), revealing a linear increase in

323　　receptive field size with an increasing vibrational frequency ($t_{(14)}$=3.24, p=0.006). However,

324　　there was no interaction effect of frequency of vibrotactile stimulation on the included

325　　Brodmann areas ($F_{(4,28)}$=0.69, p=0.606). Thus, we did not observe that receptive field sizes

326　　differed in any particular Brodmann area under differing vibrational frequency conditions.

327　　Lastly, pRF sizes also differed per preferred fingertip ($F_{(4,28)}$=6.90, p<0.001), which also

328　　exhibited a significant linear relationship between fingertip representation and pRF size

329　　($t_{(28)}$=5.13, p<0.001). Thus, pRF sizes were observed to be smallest for thumb

330　　representations and gradually increased for cortical representations of the remaining 4

331　　fingertips, with the largest receptive field sizes for the little fingertip representations (Figure

332　　5C). This effect of fingertip representation on pRF size did not differ among Brodmann areas

333　　($F_{(8,56)}$=1.32, p=0.253), or during the different frequencies of vibrotactile stimulation conditions

334　　($F_{(8,56)}$=1.40, p=0.217).

14

335

Figure 4

Title: pRF size maps

The pRF sizes are displayed on flattened cortical surfaces for all subjects (s1-s8). Rows depict the different frequencies of vibrotactile stimulation (30 Hz, 110 Hz & 190 Hz). Borders between Brodmann areas are denoted by the white solid line. The base of the central sulcus is shown by the white downward triangle, and the crown of the postcentral gyrus is indicated by the black upward triangle.

Amplitude of the BOLD signal

We found that the amplitude of the estimated percentage of BOLD signal change (*"β"*) differed significantly across the 3 Brodmann areas ($F_{(2,14)}$=8.15, p=0.004), where largest percent signal changes were measured in BA3 and gradually decreased towards BA2 ($t_{(14)}$=-4.03, p=0.001, figure 5D). However, both preferred fingertip and vibrotactile frequency did not have a significant effect on the BOLD signal amplitudes ($F_{(4,28)}$=2.21, p=0.094, and $F_{(2,14)}$=1.75, p=0.208, respectively, Figure 5E-F). Thus, the percent BOLD signal change differed per Brodmann area, but was not significantly affected by the preferred fingertip of included populations, or by the vibrotactile frequency at which fingertips were stimulated.
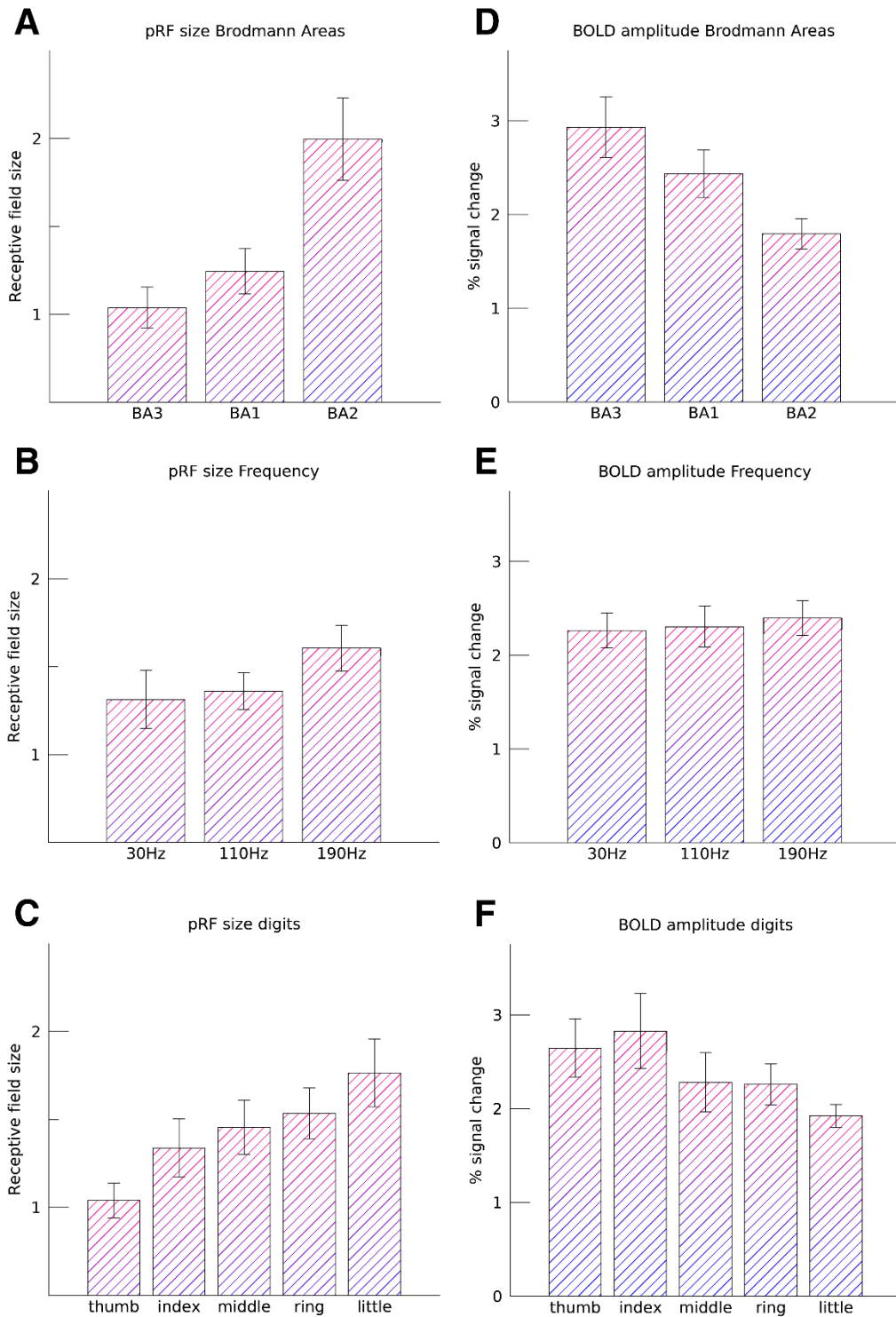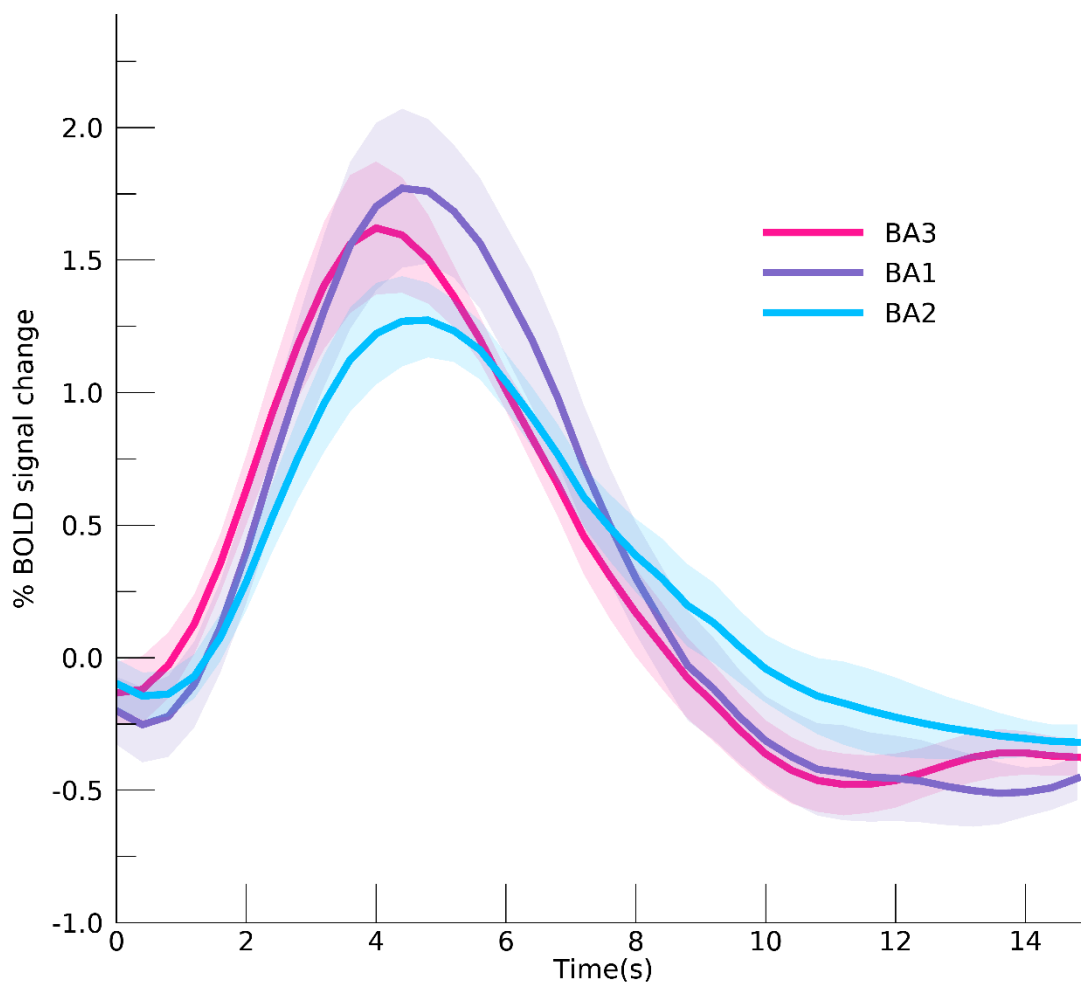
Figure 5

Title: pRF sizes and BOLD amplitudes

Figure shows the mean pRF size across subjects for Brodmann areas (A), fingertip representation (B), and vibrotactile frequency (C), as well as the corresponding estimated BOLD signal amplitude (D-F). Error bars denote the standard error of the mean across subjects.

357   *Hemodynamic response function*

358   We estimated the hemodynamic response function within S1 (figure 6). Although the largest

359   percent signal change was observed for BA1, the peak amplitude did not deviate significantly

360   across Brodmann areas ($F_{(2,12)}$=2.68, p=0.109). Neither did the FWHM of the HRFs differ

361   significantly between BA3, BA1, & BA2 ($F_{(2,12)}$=0.97, p=0.407). However, the TTP differed

362   significantly per Brodmann area ($F_{(2,12)}$=5.42, p=0.021), where the TTP in BA3 was on

363   average 0.51s (s.e.=0.17s) faster compared to the TTP seen in the other 2 Brodmann areas

364   (post-hoc t-test BA3 – BA1+BA2: $t_{(12)}$=3.07, p=0.010).

365

366   Figure 6

367   Title: Hemodynamic response functions

368   Estimated hemodynamic response functions per Brodmann area. The areas denote one standard error of the mean across
369   subjects.

370

371 **Discussion**

372 *General discussion*

373 In the current study we estimated pRFs in 3 subdivisions of human S1. The patterns of pRFs

374 can be used to suggest a cortical hierarchy among these areas, if we operationalize the

375 notion of hierarchy by the size of receptive field, specifically assuming that an area with

376 smaller pRFs is earlier in the hierarchy. We fitted a pRF model to fMRI BOLD activity in S1,

377 following vibrotactile stimulation of the fingertips. Additionally, we stimulated at 3 different

378 frequencies of vibration to investigate changes in pRF size across S1 related to

379 mechanoreceptor type and corresponding afferents. We found that pRF sizes increased from

380 BA3 to BA1 and finally BA2, consistent with the notion of a cortical hierarchy in which spatial

381 somatic information is pooled into larger and larger regions. This effect was observed under

382 all vibrotactile frequency conditions. PRF sizes also increased with higher frequency of

383 stimulation. These latter two results suggests that RA and Pacinian channels share a similar

384 cortical hierarchy, but that somatic information from a relatively larger area of the hand is

385 pooled in S1 neuronal populations during stimulation at higher frequencies. During all

386 frequencies of vibrotactile stimulation we observed a somatotopy of fingertips, despite the

387 somatotopy being less clear in BA2 compared to BA3 and BA1. No significant effect of

388 frequency on somatotopy was observed, indicating that the whole of S1 responds to

389 vibrotactile fingertip stimulation regardless of stimulation frequency. Finally, we found that

390 pRF sizes gradually increased from thumb to little finger. Neuronal populations that

391 preferentially code for the thumb responded least to stimulation of other digits, compared to

392 neuronal populations coding for the little finger, which responded to stimulation of most other

393 digits.

394 *Cortical hierarchy S1*

395 Cortical hierarchy was defined in this study through information integration, which increases

396 when information progresses higher up the processing hierarchy. Information integration is

397 associated with the widening of response profiles of neuronal populations with respect to

398 information coming from any number of possible sources. We estimated the widening of the

399 response profiles of neuronal populations with a Gaussian shaped population receptive field

400 model, where the spatial integration of somatosensory information is represented by the pRF

401 size. We find that pRF sizes differ substantially between Brodmann areas, BA3, BA1, and

402 BA2. Neuronal populations in BA3 have on average smallest pRF sizes, and the pRF sizes

403 increase along the cortical processing hierarchy towards BA1 and are largest in BA2. PRF

404 sizes in BA2 are approximately twice the size as the pRF sizes measured in BA3. This result

405 is likely analogous to the pRF size increase among cortical areas in visual cortex, where the

18

406   primary visual cortex (V1) predominantly receives thalamic output and exhibits smaller

407   receptive field sizes than visual cortical areas further up the hierarchy, as measured both at

408   the single unit level (Felleman and Van Essen 1991) and the population level with fMRI

409   (Dumoulin and Wandell 2008; Wandell and Winawer 2015), which likely reflects the average

410   receptive field size of the underlying ensemble of neurons.

411   The hierarchical order of BA3, BA1 and BA2 is further supported by a shorter time-to-

412   peak of the estimated HRF in BA3 compared to BA1 and BA2, which has also been

413   observed in magnetoencephalography (MEG) studies (Inui et al. 2004; Suzuki et al. 2013).

414   Thus, the order of cortical processing becomes apparent not merely through information

415   integration, but also in the temporal domain. However, it is important to note that both

416   feedforward and feedback neuronal processes contribute to the observed HRFs. Therefore,

417   differences in temporal components of the HRF cannot solely be attributed to differences in

418   sequential processing order. It is, for instance, possible that populations in BA1 and BA2 are

419   not merely involved in somatosensory processing at a later point in time, but also for a

420   slightly longer period of time, which would influence the observed HRF. Additionally, HRF

421   latency can be affected by non-neural processes, such as the presence of draining veins

422   (Lee et al. 1995). Nevertheless, the time-to-peak of the observed HRF in BA3 is roughly 0.5

423   seconds faster compared to the time-to-peak of the HRF in BA1 and BA2. Assuming factors

424   such as draining veins don't vary systematically between subareas in S1, this difference

425   likely has a neuronal contribution. Our findings extend animal findings to humans, and are

426   consistent with a cortical hierarchy in human S1, in which BA3 is the first cortical area to

427   receive tactile information, which is then forwarded to BA1 and BA2.

428   *Mechanoreceptive afferents*

429   We applied three frequencies of vibrotactile stimulation to the fingertips to investigate the

430   cortical hierarchy in human S1 as a result of different cutaneous mechanoreceptor afferents.

431   The 30 Hz flutter frequency most likely activated Meissner corpuscles, whereas the higher

432   frequencies would have resulted in increased contributions of Pacinian corpuscles

433   (Bolanowski et al. 1988; Johnson 2001). Regardless of the stimulated mechanoreceptor, we

434   observed somatotopic structures in all three included Brodmann areas. However, the

435   somatotopy in BA2 was less clear than in the other two areas, which likely reflects less clear

436   distinctions between cortical finger representations for areas higher up the cortical hierarchy,

437   which has been reported in a previous animal study (Iwamura et al. 1983, 1993; Pons et al.

438   1985). We did not observe that the frequency of vibrotactile stimulation influenced the

439   somatotopic structures of Brodmann areas, which may be in agreement with the notion of S1

440   neurons responding to multiple mechanoreceptor modalities (Pei et al. 2009; Abraira and

441 Ginty 2013; Saal and Bensmaia 2014). However, previous optical imaging studies in

442 monkeys have observed distinct columnar structures related to different types of

443 mechanoreceptors in BA3. (Chen et al. 2001; Friedman et al. 2004). These frequency-

444 dependent cortical columns are reportedly smaller than 400µm in size. The spatial resolution

445 used in this study was not sufficiently high to capture these differences in cortical projection

446 for different mechanoreceptor afferents.

447   Our results show that pRF sizes increase with increasing frequency of vibrotactile

448 stimulation. This effect was not found to differ across the three Brodmann areas and,

449 therefore, we find no evidence to support the notion that different mechanoreceptors types

450 project to S1 in different ways. The increase in pRF size for increased frequency could have

451 been caused by several different processes. First, cutaneous mechanoreceptive units have

452 receptive fields themselves, which could shape the feedforward information stream to S1.

453 Mechanoreceptors in glabrous skin such as the Meissner corpuscle have relatively small

454 receptive fields, whereas Pacinian corpuscles reportedly have receptive fields that extend

455 beyond the range of one finger (Bell et al. 1994; Bolanowski and Pawson 2003). Second,

456 neuronal activation thresholds could be dependent on vibrotactile frequency (Nelson et al.

457 2004; Simons et al. 2005; Ryun et al. 2017). Suprathreshold levels of activity for S1 neuronal

458 populations could be attained during stimulation of cutaneous mechanoreceptors at high

459 frequencies that would fall outside the neuronal populations' receptive fields during

460 stimulation at lower frequencies. Third, the increase in the observed pRF size for higher

461 frequencies of vibrotactile stimulation might be an extra-classical receptive field effect

462 (Friston 2005; Schwabe et al. 2006). It has been suggested that vibrotactile frequency

463 discrimination is not solely driven by mechanoreceptive afferents (Kuroki et al. 2017;

464 Birznieks et al. 2019). There may be an additional system for vibrotactile frequency

465 processing, possibly involving horizontal connections (Schwark and Jones 1989) or the

466 secondary somatosensory cortex (Nelson et al. 2004; Chung et al. 2013; Kalberlah et al.

467 2013). Further research is needed to fully characterize S1 pRF properties as a function of

468 frequency of vibrotactile stimulation.

469   In contrast to pRF size, we did not find that the amplitude of the BOLD signal was

470 significantly affected by frequency of vibrotactile stimulation despite the substantial difference

471 in kinetic energy delivered to cutaneous mechanoreceptors. Previous studies, however,

472 reported that the BOLD amplitude can either increase (Nelson et al. 2004; Goloshevsky et al.

473 2008) or decrease (Chung et al. 2013) for increasing vibrotactile frequencies of stimulation.

474 Especially when applying a vibrotactile stimulus for extended time periods, adaption

475 processes might have a negative effect on the BOLD signal amplitude. For the current

476 experiments we used an intermittent stimulation paradigm to minimize putative adaptation to

20

477   the vibrotactile stimulus. It is possible that the current stimulation duration in combination with

478   the intermittent stimulation paradigm equalized effects of different vibrotactile frequencies on

479   BOLD amplitude.

480   *Fingertip pRF size*

481   We find that fingertip representations differ in pRF size. On average, cortical representations

482   of the thumb exhibited the smallest pRF sizes, as we have reported previously (Schellekens

483   et al. 2018). A gradual increase in pRF size is observed when progressing along the

484   somatotopy, i.e. pRF size thumb < index < middle < ring < little finger. In a recent study,

485   Puckett et al. 2020 reported larger pRF sizes in S1 for little finger representations compared

486   to the index, middle and ring finger following a tactile stimulus, while measurements of the

487   thumb were not included in their study. However, they did not observe a gradual change in

488   pRF size across finger representations. The difference in results could possibly have been

489   caused by methodological differences such as the smoothing applied in their analysis, which

490   will generally increase pRF size estimates and increase the resemblance of pRF properties

491   across voxels due to the Gaussian weighted average of neighboring voxels' timeseries in

492   Gaussian smoothing algorithms. Additionally, the usage of a separately estimated HRF in our

493   study plausibly leads to better pRF estimations than using a canonical HRF as was done in

494   the study of Puckett et al. 2020.

495   The difference in pRF size across fingertips occurred in all included Brodmann areas

496   and under all vibrotactile frequency conditions. This makes it unlikely that the effect of

497   fingertip representation on pRF size reflects functional hierarchical processes. Rather, the

498   pRF size reflects the amount of integration of mechanoreceptive afferents from all fingers

499   within single neuronal populations. Thus, the differences in pRF size per fingertip

500   representation may be analogous to the increase in pRF size found in visual cortex for

501   eccentricity representations, where foveal representations display smallest pRF sizes and

502   outer eccentricities display larger pRF sizes (Smith et al. 2001; Dumoulin and Wandell 2008;

503   Harvey and Dumoulin 2011). Assuming that neuronal populations representing the fovea

504   might require high specificity for visual stimulus processing, a similar requirement may apply

505   to somatosensory processing of tactile stimulation from the thumb and index finger. The

506   thumb and index finger have the highest degree of motor acuity (Lachnit and Pieper 1990)

507   and spatial acuity for somatosensory discrimination (Vega-Bermudez and Johnson 2001).

508   Cortical pRF size might, additionally, relate to lower detection thresholds for thumb and index

509   finger compared to the other digits in tactile discrimination tasks (Tamè et al. 2014). Our

510   results indicate that neuronal populations that respond preferentially to the thumb and index

511   finger receive relatively less mechanoreceptive input from the other fingers, compared to the

512   cortical middle, ring and little finger representations, respectively.

513   *Conclusions*

514   We applied pRF modeling to investigate hierarchical information processing in S1 following

515   vibrotactile stimulation of the five fingertips. PRF modeling allows for the assessment of a

516   fingertip somatotopy in Brodmann areas BA3, BA1, and BA2. The pRF size portrays the

517   degree of spatial information integration from the five fingertips within neuronal populations of

518   cyto-architecturally distinct areas; smaller pRFs are associated with less spatial integration

519   and earlier stages of the cortical processing hierarchy. pRF sizes were smallest in BA3,

520   slightly increased for BA1, and approximately doubled in BA2, consistently across three

521   different vibration frequencies. Additionally, we observed a difference in the time course of

522   the hemodynamic response function among these Brodmann areas, with the shortest time-

523   to-peak in BA3. Our findings confirm that the cortical hierarchy of the separate Brodmann

524   areas in human S1 resembles the processing order observed in animal studies progressing

525   from BA3 to BA1 and finally BA2, independent of the activated mechanoreceptors.

526

527   **Declarations**

528   *Funding*

529   This work was supported by the National Institute Of Mental Health of the

530   National Institutes of Health under Award Number R01MH111417

531   *Conflicts of interest*

532   There are no conflicts of interest.

533   *Ethics approval*

534   This study was approved by the local medical ethics committee.

535   *Consent to participate*

536   All participants gave written informed consent prior to inclusion.

537   *Availability of data, material and code*

538   All data can be made available.

539   *Authors' contribution*

540   Conceptualization: WS, MT, SB, JW, NR, NP

541   Data acquisition: WS, MT

542   Analysis: WS, MT

543   Writing: WS

References

Abraira VE, Ginty DD (2013) The sensory neurons of touch. Neuron 79:618–639. https://doi.org/10.1016/j.neuron.2013.07.051

Akselrod M, Martuzzi R, Serino A, et al (2017) Anatomical and functional properties of the foot and leg representation in areas 3b, 1 and 2 of primary somatosensory cortex in humans: A 7T fMRI study. Neuroimage 159:473–487. https://doi.org/10.1016/j.neuroimage.2017.06.021

Ann Stringer E, Qiao PG, Friedman RM, et al (2014) Distinct fine-scale fMRI activation patterns of contra- and ipsilateral somatosensory areas 3b and 1 in humans. Hum Brain Mapp 35:4841–4857. https://doi.org/10.1002/hbm.22517

Armstrong-James M (1975) The functional status and columnar organization of single cells responding to cutaneous stimulation in neonatal rat somatosensory cortex S1. J Physiol 246:501–538

Bell J, Bolanowski S, Holmes MH (1994) The structure and function of pacinian corpuscles: A review. Prog Neurobiol 42:79–128. https://doi.org/10.1016/0301-0082(94)90022-1

Birznieks I, McIntyre S, Nilsson HM, et al (2019) Tactile sensory channels over-ruled by frequency decoding system that utilizes spike pattern regardless of receptor type. Elife 8:1–13. https://doi.org/10.7554/eLife.46510

Blankenburg F, Ruben J, Meyer R, et al (2003) Evidence for a rostral-to-caudal somatotopic organization in human primary somatosensory cortex with mirror-reversal in areas 3b and 1. Cereb Cortex 13:987–993. https://doi.org/10.1093/cercor/13.9.987

Bodegård A, Geyer S, Grefkes C, et al (2001) Hierarchical processing of tactile shape in the human brain. Neuron 31:317–328. https://doi.org/10.1016/S0896-6273(01)00362-2

Bolanowski SJ, Pawson L (2003) Organization of Meissner corpuscles in the glabrous skin of monkey and cat. Somatosens Mot Res 20:223–231. https://doi.org/10.1080/08990220310001622915

Bolanowski SJJ, Gescheider GA, Verrillo RT, Checkosky CM (1988) Four channels mediate the mechanical aspects of touch. J Acoust Soc Am 84:1680–1694

Chen LM, Friedman RM, Ramsden BM, et al (2001) Fine-scale organization of SI (area 3b) in the squirrel monkey revealed with intrinsic optical imaging. J Neurophysiol 86:3011–3029. https://doi.org/10.1152/jn.2001.86.6.3011

24

575   Choi MH, Kim SP, Kim HS, Chung SC (2016) Inter-and Intradigit Somatotopic Map of High-
576   Frequency Vibration Stimulations in Human Primary Somatosensory Cortex. Med
577   (United States) 95:1–9. https://doi.org/10.1097/MD.0000000000003714

578   Chung JM, Surmeier DJ, Lee KH, et al (1986) Classification of primate spinothalamic and
579   somatosensory thalamic neurons based on cluster analysis. J Neurophysiol 56:308–
580   327. https://doi.org/10.1152/jn.1986.56.2.308

581   Chung YG, Kim J, Han S woo, et al (2013) Frequency-dependent patterns of somatosensory
582   cortical responses to vibrotactile stimulation in humans : A fMRI study. Brain Res
583   1504:47–57. https://doi.org/10.1016/j.brainres.2013.02.003

584   Da Rocha Amaral S, Sanchez Panchuelo RM, Francis S (2019) A Data-Driven Multi-scale
585   Technique for fMRI Mapping of the Human Somatosensory Cortex. Brain Topogr.
586   https://doi.org/10.1007/s10548-019-00728-6

587   DiCarlo JJ, Johnson KO, Hsiao SS (1998) Structure of receptive fields in area 3b of primary
588   somatosensory cortex in the alert monkey. J Neurosci 18:2626–45

589   Dijkerman HC, de Haan EHF (2007) Somatosensory processes subserving perception and
590   action. Behav Brain Sci 30:189–201. https://doi.org/10.1017/S0140525X07001392

591   Duffy FH, Burchfiel JL (1971) Somatosensory System: Organizational Hierarchy from Single
592   Units in Monkey Area 5. Am Assoc Adv Sci 172:273–275

593   Dumoulin SO, Hess RF, May KA, et al (2014) Contour extracting networks in early
594   extrastriate cortex. J Vis 14(5):1–14. https://doi.org/10.1167/14.5.18.doi

595   Dumoulin SO, Wandell BA (2008) Population receptive field estimates in human visual
596   cortex. Neuroimage 39:647–60. https://doi.org/10.1016/j.neuroimage.2007.09.034

597   Felleman DJ, Van Essen DC (1991) Distributed hierarchical processing in the primate
598   cerebral cortex. Cereb Cortex 1:1–47. https://doi.org/10.1093/cercor/1.1.1

599   Fischl B, Rajendran N, Busa E, et al (2008) Cortical folding patterns and predicting
600   cytoarchitecture. Cereb Cortex 18:1973–1980. https://doi.org/10.1093/cercor/bhm225

601   Friedman DP (1983) Laminar patterns of termination of cortico-cortical afferents in the
602   somatosensory system. Brain Res. https://doi.org/10.1016/0006-8993(83)91103-4

603   Friedman RM, Chen LM, Roe AW (2004) Modality maps within primate somatosensory
604   cortex. Proc Natl Acad Sci U S A 101:12724–12729.

605   https://doi.org/10.1073/pnas.0404884101

606   Friston K (2005) A theory of cortical responses. Philos Trans R Soc B Biol Sci 360:815–836.
607   https://doi.org/10.1098/rstb.2005.1622

608   Gescheider GA, Bolanowski SJ, Verrillo RT (2004) Some characteristics of tactile channels.
609   Behav Brain Res 148:35–40. https://doi.org/10.1016/S0166-4328(03)00177-3

610   Goloshevsky AG, Silva AC, Dodd SJ, Koretsky AP (2008) BOLD fMRI and Somatosensory
611   Evoked Potentials Are Well Correlated Over a Broad Range of Frequency Content of
612   Somatosensory Stimulation of the Rat Forepaw. Brain Res 1195:67–76.
613   https://doi.org/10.1038/jid.2014.371

614   Haak K V., Cornelissen FW, Morland AB (2012) Population receptive field dynamics in
615   human visual cortex. PLoS One 7:1–8. https://doi.org/10.1371/journal.pone.0037686

616   Harvey BM, Dumoulin SO (2011) The relationship between cortical magnification factor and
617   population receptive field size in human visual cortex: constancies in cortical
618   architecture. J Neurosci 31:13604–12. https://doi.org/10.1523/JNEUROSCI.2572-
619   11.2011

620   Harvey MA, Saal HP, Dammann JF, Bensmaia SJ (2013) Multiplexing Stimulus Information
621   through Rate and Temporal Codes in Primate Somatosensory Cortex. PLoS Biol 11:.
622   https://doi.org/10.1371/journal.pbio.1001558

623   Herron P, Dykes R (1986) The ventroposterior inferior nucleus in the thalamus of cats: A
624   relay nucleus in the Pacinian pathway to somatosensory cortex. J Neurophysiol
625   56:1475–1497. https://doi.org/10.1152/jn.1986.56.6.1475

626   Hlustík P, Solodkin a, Gullapalli RP, et al (2001) Somatotopy in human primary motor and
627   somatosensory hand representations revisited. Cereb Cortex 11:312–321.
628   https://doi.org/10.1093/cercor/11.4.312

629   Hubel DH, Wiesel TN (1968) Receptive fields and functional architecture of monkey striate
630   cortex. J Physiol 195:215–243

631   Hyvärinen J, Poranan A (1978) Receptive field integration and submodality convergence in
632   the hand area of the post-central gyrus of the alert monkey. J Physiol 283:539–556

633   Inui K, Wang X, Tamura Y, et al (2004) Serial processing in the human somatosensory
634   system. Cereb Cortex 14:851–857. https://doi.org/10.1093/cercor/bhh043

635 Iwamura Y (1998) Hierarchical somatosensory processing. Curr Opin Neurobiol 8:522–528.
636   https://doi.org/10.1016/S0959-4388(98)80041-X

637 Iwamura Y, Tanaka M, Sakamoto M, Hikosaka O (1983) Functional subdivisions
638   representing different finger regions in area 3 of the first somatosensory cortex of the
639   conscious monkey. Exp Brain Res 51:315–326

640 Iwamura Y, Tanaka M, Sakamoto M, Hikosaka O (1993) Rostrocaudal gradients in the
641   neuronal receptive field complexity in the finger region of the alert monkey's postcentral
642   gyrus. Exp Brain Res 92:360–368. https://doi.org/10.1007/BF00229023

643 Johnson KO (2001) The roles and functions of cutaneous mechanoreceptors. Curr Opin
644   Neurobiol 11:455–461. https://doi.org/10.1016/S0959-4388(00)00234-8

645 Jones EG, Powell TPS (1970) Connexions of the somatic sensory cortex of the rhesus
646   monkey: III.-Thalamic connexions. Brain 93:37–56. https://doi.org/10.1093/brain/93.1.37

647 Kaas JH (1993) The functional organization of somatosensory cortex in primates. Ann Anat
648   175:509–518. https://doi.org/10.1016/S0940-9602(11)80212-8

649 Kalberlah C, Villringer A, Pleger B (2013) Dynamic causal modeling suggests serial
650   processing of tactile vibratory stimuli in the human somatosensory cortex-An fMRI
651   study. Neuroimage 74:164–171. https://doi.org/10.1016/j.neuroimage.2013.02.018

652 Kikkert S, Kolasinski J, Jbabdi S, et al (2016) Revealing the neural fingerprints of a missing
653   hand. Elife 5:1–19. https://doi.org/10.7554/eLife.15292

654 Kim J, Müller KR, Chung YG, et al (2015) Distributed functions of detection and
655   discrimination of vibrotactile stimuli in the hierarchical human somatosensory system.
656   Front Hum Neurosci 8:1–10. https://doi.org/10.3389/fnhum.2014.01070

657 Klein BP, Harvey BM, Dumoulin SO (2014) Attraction of Position Preference by Spatial
658   Attention throughout Human Visual Cortex. Neuron 84:227–237.
659   https://doi.org/10.1016/j.neuron.2014.08.047

660 Kolasinski J, Makin TR, Jbabdi S, et al (2016) Investigating the Stability of Fine-Grain Digit
661   Somatotopy in Individual Human Participants. J Neurosci 36:1113–1127.
662   https://doi.org/10.1523/JNEUROSCI.1742-15.2016

663 Kuroki S, Watanabe J, Nishida S (2017) Integration of vibrotactile frequency information
664   beyond the mechanoreceptor channel and somatotopy. Sci Rep 7:1–13.
665   https://doi.org/10.1038/s41598-017-02922-7

666   Kurth R, Villringer K, Curio G, et al (2000) fMRI shows multiple somatotopic digit
667   representations in human primary somatosensory cortex. Neuroreport 11:1487–1491.
668   https://doi.org/10.1097/00001756-200005150-00026

669   Lachnit H, Pieper W (1990) Speed and accuracy effects of fingers and dexterity in 5-choice
670   reaction tasks. Ergonomics 33:1443–1454. https://doi.org/10.1080/00140139008925345

671   Lee AT, Glover GH, Meyer CH (1995) Discrimination of Large Venous Vessels in Time-
672   Course Spiral Blood-Oxygen-Level-Dependent Magnetic-Resonance Functional
673   Neuroimaging. Magn Reson Med. https://doi.org/10.1002/mrm.1910330602

674   Lindquist MA, Meng Loh J, Atlas LY, Wager TD (2009) Modeling the hemodynamic response
675   function in fMRI: efficiency, bias and mis-modeling. Neuroimage 45:S187–S198.
676   https://doi.org/10.1016/j.neuroimage.2008.10.065

677   Maldjian JA, Gottschalk A, Patel RS, et al (1999) The sensory somatotopic map of the
678   human hand demonstrated at 4 Tesla. Neuroimage 10:55–62.
679   https://doi.org/10.1006/nimg.1999.0448

680   Markwardt CB (2009) Non-linear Least-squares Fitting in IDL with MPFIT. Astron Data Anal
681   Softw Syst XVIII ASP Conf Ser 411:251. https://doi.org/citeulike-article-id:4067445

682   Martuzzi R, van der Zwaag W, Farthouat J, et al (2014) Human finger somatotopy in areas
683   3b, 1, and 2: A 7T fMRI study using a natural stimulus. Hum Brain Mapp 35:213–226.
684   https://doi.org/10.1002/hbm.22172

685   Merkel C, Hopf JM, Schoenfeld MA (2018) Spatial elongation of population receptive field
686   profiles revealed by model-free fMRI back-projection. Hum Brain Mapp 39:2472–2481.
687   https://doi.org/10.1002/hbm.24015

688   Miller KD, Pinto DJ, Simons DJ (2001) Processing in layer 4 of the neocortical circuit: New
689   insights from visual and somatosensory cortex. Curr Opin Neurobiol 11:488–497.
690   https://doi.org/10.1016/S0959-4388(00)00239-7

691   Mountcastle VB, LaMotte RH, Giancarlo C (1972) Detection thresholds for stimuli in humans
692   and monkeys: Comparison with threshold events in mechanoreceptive afferent nerve
693   fibers innervating the monkey hand. J Neuroimaging 35:122–136

694   Nelson AJ, Chen R (2008) Digit somatotopy within cortical areas of the postcentral gyrus in
695   humans. Cereb Cortex 18:2341–2351. https://doi.org/10.1093/cercor/bhm257

696   Nelson AJ, Staines WR, Graham SJ, McIlroy WE (2004) Activation in SI and SII; The

697   influence of vibrotactile amplitude during passive and task-relevant stimulation. Cogn
698   Brain Res 19:174–184. https://doi.org/10.1016/j.cogbrainres.2003.11.013

699 Pasterkamp E (1999) Mechanoreceptors in the glabrous skin of the human hand. Arch
700   Physiol Biochem 107:338–341. https://doi.org/10.1076/13813455199908107041qft338

701 Paul RL, Merzenich M, Goodman H (1972) Representation of slowly and rapidly adapting
702   cutaneous mechanoreceptors of the hand in brodmann's areas 3 and 1 of Macaca
703   Mulatta. Brain Res 36:229–249. https://doi.org/10.1016/0006-8993(72)90732-9

704 Pei YC, Denchev P V., Hsiao SS, et al (2009) Convergence of submodality-specific input
705   onto neurons in primary somatosensory cortex. J Neurophysiol 102:1843–1853.
706   https://doi.org/10.1152/jn.00235.2009

707 Pons TP, Garraghty PE, Cusick CG, Kaas JH (1985) The somatotopic organization of area 2
708   in macaque monkeys. J Comp Neurol. https://doi.org/10.1002/cne.902410405

709 Puckett AM, Bollmann S, Junday K, et al (2020) Bayesian population receptive field modeling
710   in human somatosensory cortex. Neuroimage 208:116465.
711   https://doi.org/10.1016/j.neuroimage.2019.116465

712 Rowe MJ (2002) Synaptic transmission between single tactile and kinaesthetic sensory
713   nerve fibers and their central target neurones. Behav Brain Res 135:197–212.
714   https://doi.org/10.1016/S0166-4328(02)00166-3

715 Ryun S, Kim JS, Lee H, Chung CK (2017) Tactile Frequency-Specific High-Gamma Activities
716   in Human Primary and Secondary Somatosensory Cortices. Sci Rep 7:1–10.
717   https://doi.org/10.1038/s41598-017-15767-x

718 Saal HP, Bensmaia SJ (2014) Touch is a team effort: Interplay of submodalities in cutaneous
719   sensibility. Trends Neurosci 37:689–697. https://doi.org/10.1016/j.tins.2014.08.012

720 Saal HP, Harvey MA, Bensmaia SJ (2015) Rate and timing of cortical responses driven by
721   separate sensory channels. Elife 4:1–16. https://doi.org/10.7554/eLife.10450

722 Sánchez-Panchuelo RM, Besle J, Mougin O, et al (2014) Regional structural differences
723   across functionally parcellated Brodmann areas of human primary somatosensory
724   cortex. Neuroimage 93:221–230. https://doi.org/10.1016/j.neuroimage.2013.03.044

725 Sanchez-Panchuelo RM, Francis S, Bowtell R, Schluppeck D (2010) Mapping human
726   somatosensory cortex in individual subjects with 7T functional MRI. J Neurophysiol
727   103:2544–2556. https://doi.org/10.1152/jn.01017.2009

728   Sanchez Panchuelo RM, Besle J, Schluppeck D, et al (2018) Somatotopy in the Human
729   Somatosensory System. Front Hum Neurosci 12:1–14.
730   https://doi.org/10.3389/fnhum.2018.00235

731   Schellekens W, Petridou N, Ramsey NF (2018) Detailed somatotopy in primary motor and
732   somatosensory cortex revealed by Gaussian population receptive fields. Neuroimage
733   179:337–347. https://doi.org/10.1016/j.neuroimage.2018.06.062

734   Schwabe L, Obermayer K, Angelucci A, Bressloff PC (2006) The role of feedback in shaping
735   the extra-classical receptive field of cortical neurons: A recurrent network model. J
736   Neurosci 26:9117–9129. https://doi.org/10.1523/JNEUROSCI.1253-06.2006

737   Schwark HD, Jones EG (1989) The distribution of intrinsic cortical axons in area 3b of cat
738   primary somatosensory cortex. Exp Brain Res 78:501–513.
739   https://doi.org/10.1007/BF00230238

740   Schweizer R, Voit D, Frahm J (2008) Finger representations in human primary
741   somatosensory cortex as revealed by high-resolution functional MRI of tactile
742   stimulation. Neuroimage 42:28–35. https://doi.org/10.1016/j.neuroimage.2008.04.184

743   Simons SB, Tannan V, Chiu J, et al (2005) Amplitude-dependency of response of SI cortex
744   to flutter stimulation. BMC Neurosci 6:1–14. https://doi.org/10.1186/1471-2202-6-43

745   Smith AT, Singh KD, Williams AL, Greenlee MW (2001) Estimating receptive field size from
746   fMRI data in human striate and extrastriate visual cortex. Cereb Cortex 11:1182–90

747   Sur M, Merzenich MM, Kaas JH (1980) Magnification, receptive-field area, and
748   "hypercolumn" size in areas 3b and 1 of somatosensory cortex in owl monkeys. J
749   Neurophysiol 44:295–311. https://doi.org/10.1152/jn.1980.44.2.295

750   Suzuki M, Wasaka T, Inui K, Kakigi R (2013) Reappraisal of field dynamics of motor cortex
751   during self-paced finger movements. Brain Behav 3:747–762.
752   https://doi.org/10.1002/brb3.186

753   Tal Z, Geva R, Amedi A (2017) Positive and Negative Somatotopic BOLD Responses in
754   Contralateral Versus Ipsilateral Penfield Homunculus. Cereb Cortex 27:962–980.
755   https://doi.org/10.1093/cercor/bhx024

756   Tamè L, Moles A, Holmes NP (2014) Within, but not between hands interactions in
757   vibrotactile detection thresholds reflect somatosensory receptive field organization.
758   Front Psychol 5:1–9. https://doi.org/10.3389/fpsyg.2014.00174

759 Vallbo AB, Johansson RS (1984) Properties of cutaneous mechanoreceptors in the human
760   hand related to touch sensation. Hum Neurobiol 3:3–14

761 Van Boven RW, Ingeholm JE, Beauchamp MS, et al (2005) Tactile form and location
762   processing in the human brain. Proc Natl Acad Sci U S A 102:12601–12605.
763   https://doi.org/10.1073/pnas.0505907102

764 Van de Moortele P-F, Auerbach EJ, Olman C, et al (2009) T1 weighted brain images at 7
765   Tesla unbiased for proton density, T2* contrast and RF coil receive B1 sensitivity with
766   simultaneous vessel visualization. Neuroimage 46:432–446.
767   https://doi.org/10.1016/j.neuroimage.2009.02.009.T

768 Van Essen DC, Maunsell JHR (1983) Hierarchical organization and functional streams in the
769   visual cortex. Trends Neurosci 6:370–375

770 Vega-Bermudez F, Johnson KO (2001) Differences in spatial acuity between digits.
771   Neurology. https://doi.org/10.1212/WNL.56.10.1389

772 Wagstyl K, Ronan L, Goodyer IM, Fletcher PC (2015) Cortical thickness gradients in
773   structural hierarchies. Neuroimage 111:241–250.
774   https://doi.org/10.1016/j.neuroimage.2015.02.036

775 Wandell BA, Winawer J (2015) Computational neuroimaging and population receptive fields.
776   Trends Cogn Sci 19:349–357. https://doi.org/10.1016/j.tics.2015.03.009

777 Welbourne LE, Morland AB, Wade AR (2018) Population receptive field (pRF)
778   measurements of chromatic responses in human visual cortex using fMRI. Neuroimage
779   167:84–94. https://doi.org/10.1016/j.neuroimage.2017.11.022

780 Whitehead K, Papadelis C, Laudiano-Dray MP, et al (2019) The emergence of hierarchical
781   somatosensory processing in late prematurity. Cereb Cortex 29:2245–2260.
782   https://doi.org/10.1093/cercor/bhz030

783

784

785 **Figure legends**

786 Figure 1

787 pRF model timeseries

788 (A) Figure shows the effect of increasing pRF size on modeled timeseries. Left image shows
789 model with pRF center = 1 (index finger, yellow bar), pRF size = 0.5 (finger units). Middle
790 image: pRF center = 1, pRF size = 1.5. Right image: pRF center = 1, pRF size = 2.5. The
791 model timeseries are convolved with the average HRF from the HRF experiment and the
792 colored bars denote the model onset time for each of the fingertip conditions, see hand icon.
793 (B) Fitted pRF timeseries (black) for one example vertex and the corresponding acquired
794 fMRI timeseries (pink) are shown. For visibility, only a part of the complete timeseries is
795 shown. The onsets of the fingertip stimulation conditions are represented by the colored
796 bars, see also hand icon. This particular vertex was acquired from subject 4, BA1, 190 Hz,
797 and was fitted with a model with pRF center= 2.74 (between index and middle finger) and
798 pRF size = 1.70 finger units.

799 Figure 2

800 Title: Fingertip somatotopy

801 (A) Single subject pRF centers following 190 Hz vibrotactile stimulation are presented on a
802 pial surface and flattened surface (circle). The cortical coordinates along the dorsoventral
803 axis plotted against the pRF centers are shown for all three Brodmann areas. For the pRF
804 centers, 1=thumb, 2=index finger, 3=middle finger, 4=ring finger, 5=little finger, which is also
805 indicated by the colors in the scatterplot and the hand icon. (B) Group average of cortical
806 coordinates along the dorsoventral axis plotted against the mean pRF center per fingertip
807 1=thumb, 2=index finger, 3=middle finger, 4=ring finger, 5=little finger). Shaded area
808 represents standard error of the mean across subjects. Different symbols represent different
809 vibrational frequencies.

810

811 Figure 3

812 Title: pRF center maps

813 The pRF centers are displayed on flattened cortical surfaces for all subjects (s1-s8). Rows
814 depict the different frequencies of vibrotactile stimulation (30 Hz, 110 Hz & 190 Hz). Borders
815 between Brodmann areas are denoted by the white solid line. The base of the central sulcus

32

816   is shown by the white downward triangle, and the crown of the postcentral gyrus is indicated

817   by the black upward triangle. Correspondence of pRF center and fingertip is denoted by the

818   hand icon.

819

820   Figure 4

821   Title: pRF size maps

822   The pRF sizes are displayed on flattened cortical surfaces for all subjects (s1-s8). Rows

823   depict the different frequencies of vibrotactile stimulation (30 Hz, 110 Hz & 190 Hz). Borders

824   between Brodmann areas are denoted by the white solid line. The base of the central sulcus

825   is shown by the white downward triangle, and the crown of the postcentral gyrus is indicated

826   by the black upward triangle.

827

828   Figure 5

829   Title: Average pRF sizes and BOLD amplitudes

830   Figure shows the average pRF size across subjects for Brodmann areas (A), fingertip

831   representation (B), and vibrotactile frequency (C), as well as the corresponding estimated

832   BOLD signal amplitude (D-F). Error bars denote the standard error of the mean across

833   subjects.

834

835   Figure 6

836   Title: Hemodynamic response functions

837   Estimated hemodynamic response functions per Brodmann area. The areas denote one

838   standard error of the mean across subjects.

839

840

841